inter.noise
HAMBURG 2016

Payload Fill Effect Investigation of a Large Launch Vehicle Fairing

Ling ZHENG[1]; Yuanyuan CHEN[1]; Shuhong XIANG[2]; Guiqian FANG[2]; Ye LI[2]; Jiang YANG[2]

[1] State Key Laboratory of Mechanical Transmission, College of Automotive Engineering, Chongqing University, Chongqing

[2] Beijing Institute of Spacecraft Environment Engineering, Beijing

ABSTRACT

About the phenomenon of local SPL (Sound Pressure Level) increase caused by the payload filled in the launch vehicle fairing (fill effect problem), equivalent models of the fairing and payloads are established using the sandwich plate theory. The interior acoustic characteristic of the fairing is simulated through FE-BEM (Finite Element-Boundary Element Method) and SEA (Statistical Energy Analysis) method, and the fill effects of two payloads with different volume ratio are analyzed contrastively. Besides, the mechanism and distribution characteristic of fill effect are studied from the point of mode frequencies shift. The simulation and test results show that fill effect is associated with acoustic mode frequencies shift caused by sound-vibration coupling. The shift ratio is greater at low frequencies than high frequencies, which makes the fill effect more obvious. For the payload fill factor can influence shift ratio, fill effect will increase as fill factor increases. Numerical computation method based on FE-BEM and SEA provide an effective way to predict the payload fill effect.

Keywords: Fairing, Payload, Sound Pressure Level, Fill Effect
I-INCE Classification of Subjects Number(s): 75

1. INTRODUCTION

During a rocket launch, the acoustic field in the fairing becomes very severe due to the high-speed jet noise and aerodynamic noise of rocket engine. In acoustic tests, local pressure increase in the narrow gap between the payload and the fairing is often seen, which can be over 10dB.This phenomenon is called as the fill effect due to the payloads filled in the fairing. The fill effect is proved to be a function of the fill factor (the volume ratio of a payload to the fairing or cargo) and frequency. Often, the acoustic environment defined in aerospace field is representative of the unfilled (empty cargo or fairing without payload) environment. Therefore, it becomes necessary to take into account the payload fill and its effects on the interior SPL since the sound field distribution will be changed.

Early in 1980's, a series of researches have been examined by NASA on the problem of fill effect. The effects on SPL in the fairing resulted by payloads filling of four different shapes, sizes and volumes were tested. Then based on these tests, a theoretical model was proposed to predict fill effect based on the results of these tests and the industry standard NASA-STD-7001A was developed [1]. However, this prediction equation is of poor ability at low frequencies. Terry investigated the effect of fill factor on interior acoustic filed of the firing by using SEA (Statistical Energy Approach) method [2]. This study shows that the fill factor is a fact for the cavity SPL's, but (may be) friction for predicting the spacecraft response. FEM (Finite Element Method) and BEM (Boundary Element Method) are used to clarify the mechanism and evaluate this pressure increase [3]. It is found that the main reason of the phenomenon is dominated by the acoustic cavity on the appropriate boundary condition rather than structure vibration. And it is clear that the local sound pressure level increase will increase the vibration proportionally of the structure adjoin the acoustic cavity. Besides, it is verified that the payload geometry could play a significant role in determining the acoustic pressure inside the fairing [4, 5].

Obviously, although fill effect have been studied from different perspectives, the existing

[1] zling@cqu.edu.cn
[2] jx_41040118@163.com

theoretical prediction model is not as ideal as expected at low frequencies. A more accurate theoretical or numerical method is in urgent need to predict the fill effect at low frequencies or full-band frequencies, and to provide theoretical basis for further modification on NASA-STD-7001A.

In this paper, FE-BEM and SEA method are applied to study the fill effect of a payload fairing and the fill effects of two payloads with different volume ratio are simulated, aiming to reveal the mechanism and distribution characteristics of fill effect and provide theoretical basis for the fill effect prediction and the revision of acoustic test standard.

2. NUMERICAL ANALYSIS MODELS

2.1 Equivalent Treatment of Honeycomb Structure Fairing

Honeycomb sandwich structures are usually composed of the upper and lower skin layer and the intermediate honeycomb core, as Figure 1(a) shows. Such structures have been widely used in aerospace and other fields, due to its high specific strength, stiffness ratio, good insulation isolation performance and many other advantages. The test fairing and payloads in this paper are made up of regular hexagon aluminum honeycomb sandwich structures. It contains too many degrees of freedom which will cause excessive number of grids and affect the calculation efficiency, considering that the aluminum foil hive is very thin and there is a large amount of hive. So it is necessary to take equivalent ways to deal with honeycomb structure.

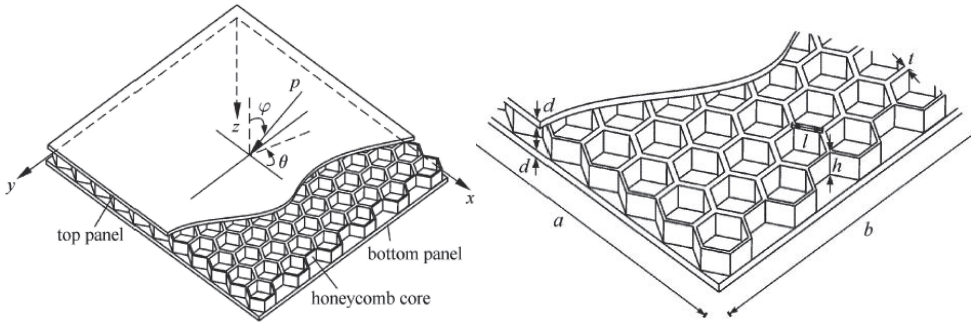

(a) Global view (b) Partial enlarged view

Figure 1 - Honeycomb sandwich structure

The current equivalent theories used in engineering include: sandwich panel theory [6, 7], equivalent plate theory [8, 9] and honeycomb plate theory [10]. Only honeycomb core is equivalent to a homogeneous layer in sandwich panel theory. The honeycomb sandwich structure is equivalent to an isotropic plate with different thickness in the equivalent plate theory. It is equivalent to an orthotropic plate with the same size in honeycomb plate theory. Here, sandwich panel theory is adopted, which is considered more accuracy and less computing cost. For honeycomb sandwich panels with regular hexagon honeycomb core, the elastic constants of the equivalent layer and original material satisfy the following relation [12],

$$\begin{cases} E_x = \dfrac{4}{\sqrt{3}} E_c \left(1 - 3\dfrac{t^2}{l^2}\right)\dfrac{t^3}{l^3} \\ E_z = \dfrac{8\sqrt{3}}{9} E_c \dfrac{t}{l} \\ E_y = \dfrac{4}{\sqrt{3}} E_c \left(1 - \dfrac{5}{3}\dfrac{t^2}{l^2}\right)\dfrac{t^3}{l^3} \\ G_{xz} = \dfrac{\sqrt{3}}{3} G_c \dfrac{t}{l} \\ G_{xy} = \dfrac{4\sqrt{3}}{5} E_c \left(1 - \dfrac{12}{5}\dfrac{t^2}{l^2}\right)\dfrac{t^3}{l^3} \\ G_{yz} = \dfrac{2\sqrt{3}}{3} G_s \dfrac{t}{l} \\ \rho = \dfrac{8}{3\sqrt{3}}\dfrac{t}{l}\rho_c \quad \mu_{xy} = 1 - \dfrac{4t^2}{l^2} \\ \mu_{yx} = 1 - \dfrac{8t^2}{3l^2} \quad \mu_{zx} = \mu_{zy} = \mu_c \\ \mu_{xz} = \mu_{zx}\dfrac{E_{xz}}{E_{zx}} \quad \mu_{yz} = \mu_{zy}\dfrac{E_{yz}}{E_{zy}} \end{cases} \tag{1}$$

In the above formulas, t is the thickness of honeycomb wall, l is the side length of regular hexagon, as shown in Figure 1 (b). ρ_c, μ_c, E_c, G_c are the density, Poisson's ratio, elastic modulus and shear modulus of the original core respectively, and ρ, μ_{ij}, E_{ij}, G_{ij} are the density, Poisson's ratio, elastic modulus and shear modulus of the equivalent layer respectively. The followings are the parameters of the occupied honeycomb sandwich structure in this paper, and the equivalent parameters are shown in Table 1.

For the top/bottom aluminum panel,

$$E_f = 68\text{GPa},\ \mu_f = 0.34,\ \rho_f = 2700\text{kg/m}^3,\ d = 0.5\text{mm}$$

For the honeycomb core,

$$l = 5mm,\ t = 0.05mm,\ h = 28mm,\ \mu_c = 0.34,\ \rho_c = 2450\text{kg/m}^3,\ E_c = 68\text{GPa}$$

Table 1 - Equivalent parameters of honeycomb core

Equivalent Parameter	Values	Equivalent Parameter	Values
E_x	0.15 MPa	G_{zx}	306 MPa
E_y	0.15 MPa	μ_{xy}	0.996
E_z	1000 MPa	μ_{yz}	5.1e-5
G_{xy}	0.09 MPa	μ_{zx}	0.34
G_{yz}	153 MPa	ρ	37.7 kg/m^3

2.2 FE/BE Analysis Model

2.2.1 Coupled FE/Indirect BE Analysis Method

The finite element method (FEM) is usually applied to predict structural response, while boundary element method (BEM) can be used to calculate acoustic response. For coupled vibro-acoustic problems, a combination of FEM and BEM is necessary to obtain structural and acoustic response.

BEM includes direct and indirect BEM [13], the fluid in direct BEM must be closed cavity and can only be on one side of the element, while the fluid in indirect BEM can be closed or not and both sides are allowed. Since the interior and exterior sound field can be considered simultaneously in indirect BEM, indirect boundary element method is used here to establish the coupled vibro-acoustic model.

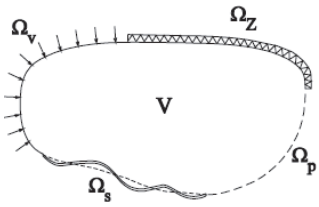

Figure 2 - coupled vibro-acoustic system

For coupled vibro-acoustic system showed in Figure 2, the closed fluid domain V contains four different boundary conditions. Ω_p, Ω_v, Ω_Z are the imposed pressure, normal velocity and normal impedance surface respectively. Supposing that $\Omega_\sigma = \Omega_p$, $\Omega_\mu = \Omega_v \cup \Omega_Z$, the boundary element approximations of the steady-state on the boundary surface $\Omega_a = \Omega_\sigma \cup \Omega_\mu$ of a fluid domain are $\hat{\sigma}$ and $\hat{\mu}$ in terms of a set of global shape functions,

$$\hat{\sigma}(\vec{r_a}) = [N_\sigma] \cdot \{\hat{\sigma}_i\}, \quad (\vec{r_a}) \in \Omega_\sigma \tag{2}$$

$$\hat{\mu}(\vec{r_a}) = [N_\mu] \cdot \{\hat{\mu}_i\}, \quad (\vec{r_a}) \in \Omega_\mu \tag{3}$$

where $[N_\sigma]$ and $[N_\mu]$ are matrices of global shape functions, associated with the nodes on the boundary surface Ω_σ and Ω_μ respectively. $\{\hat{\sigma}_i\}$ and $\{\hat{\mu}_i\}$ comprise the nodal single and double layer potentials. In absence of any external acoustic source, the resulting indirect BE model takes the form,

$$\begin{bmatrix} B & C \\ C^T & D \end{bmatrix} \cdot \begin{Bmatrix} \hat{\sigma}_i \\ \hat{\mu}_i \end{Bmatrix} = \begin{Bmatrix} \tilde{f}_\sigma \\ \tilde{f}_\mu \end{Bmatrix} \tag{4}$$

On the surface of Ω_σ, the finite element approximations of displacement in the x-, y- and z-direction of a global Cartesian co-ordinate system are

$$\begin{Bmatrix} \hat{w}_x(x,y,z) \\ \hat{w}_y(x,y,z) \\ \hat{w}_z(x,y,z) \end{Bmatrix} = [N_s] \cdot \{w_i\} + [N_{\bar{w}}] \cdot \{\bar{w}_i\} \tag{5}$$

where $[N_s]$ and $[N_{\bar{w}}]$ are matrices of global shape functions, $\{w_i\}$ and $\{\bar{w}_i\}$ are displacement vectors. The resulting finite element model is

$$([K_s] + j\omega[C_s] - \omega^2[M_s]) \cdot \{w_i\} = [F_s] \tag{6}$$

The matrices $[K_s]$, $[C_s]$ and $[M_s]$ are structure stiffness, damping and mass matrices. $[F_s]$ is the load vector of the structure model.

Considering the interaction on the fluid-structural coupling interface in a coupled vibro-acoustic system, an additional coupling term must be added to equation (4) and (6). Combining the modified structural FE model and the modified acoustic BE model yields the coupled FE/indirect BE model

$$\begin{bmatrix} K_s + j\omega C_s - \omega^2 M_s & L_c \\ {L_c}^T & \dfrac{D}{\rho_0 \omega^2} \end{bmatrix} \cdot \begin{Bmatrix} w_i \\ \hat{\mu}_i \end{Bmatrix} = \begin{Bmatrix} F_s \\ F_a \end{Bmatrix} \tag{7}$$

where L_c is the coupling matrix, D is the IBEM impact matrix and $[F_a]$ is the load vector of the fluid model. It can be seen from equation (7) that the displacement of the structure finite element and the pressure of the acoustic boundary element are coupled together due to L_c coupling matrix. Therefore, it is possible to impose vibration and noise load at the same time and achieve the coupling solutions.

2.2.2 FE/BE Model

Acoustic-structural coupling models are established using LMS Virtual Lab for the numerical computation of fill effect at low frequencies. Fig.3 shows the finite element models of different fairing /payload combination. The grid type is hexahedral, the size of which is controlled in 100mm considering the calculation accuracy and efficiency. As required, the satellite brackets and adapter brackets (Here in after referred to as the brackets) are included in the empty fairing. The fill factor (the ratio of the payload volume

to the empty fairing volume in the same length at the cylindrical section) of the large and small payload are 35.77% and 28.0575% respectively. The involved frequency range is 31.5Hz~250Hz (band-center frequency).

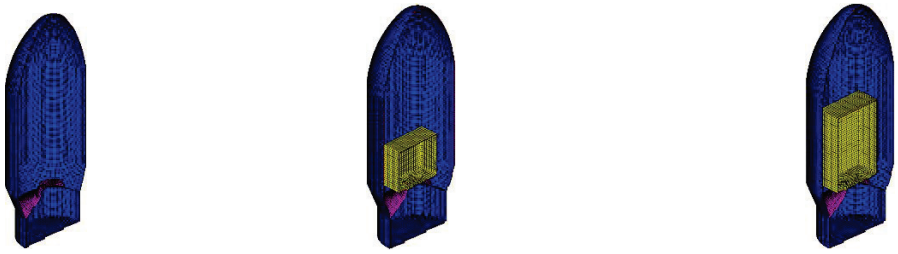

(a)Empty fairing (b) Fairing with small payload (c) Fairing with large payload

Figure 3 - FE models of fairing/payload combinations

Figure 4 shows the acoustic boundary element models, the grid type in this model is quadrilateral in two-dimensional. The grid size is limited to 200mm to ensure 6 elements in the minimum wavelength of the calculating frequency range. The air cavity in the empty fairing is divided into two parts: one is formed by the fairing and brackets and the other is formed by the brackets and instrument cabin. While the air cavity in the filled fairing comprises three parts: one is formed by the fairing, payload and brackets; another is formed by the brackets and instrument cabin; and the last one is inside the payload.

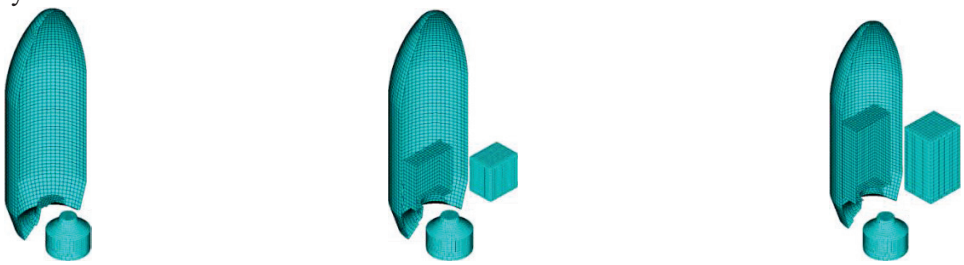

(a)Empty fairing (b) Fairing with small payload (c) Fairing with large payload

Figure 4 - Acoustic boundary element models

Distributed plane wave is applied as acoustic excitation to build the required reverberant acoustic field. Distributed plane wave reverberant field is shown in Figure 5, the sound pressure levels (SPL) from experimental measurement are used as acoustic excitation in reverberant field.

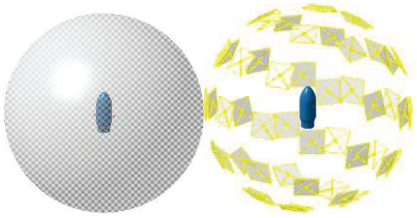

Figure 5 - Spatial distribution of distributed plane waves

2.3 SEA Analysis Model

2.3.1 SEA Analysis Method

SEA is a statistical analysis method which uses energy flow to assess the system dynamic characteristics, vibration response and acoustic radiation theoretically. Figure 6 shows the coupling power flow relationship between two subsystems. They are as follows:

$$p_1 = \omega\eta_1 E_1 + \omega\eta_{12} E_1 - \omega\eta_{21} E_2 \tag{8}$$

$$p_2 = \omega\eta_2 E_2 + \omega\eta_{21} E_2 - \omega\eta_{12} E_1 \tag{9}$$

where ω is the band-center frequency, η_{12} is the coupling loss factor stands for the energy from subsystem 1 to subsystem 2 and η_{21} is that of the reverse.

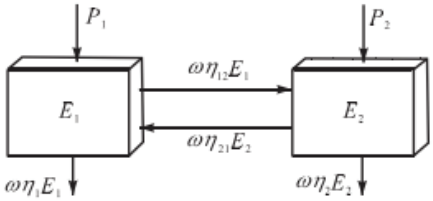

Figure 6 - Power flow relationship between two subsystems

For a conservative system, power flow shows reversibility. Therefore, the modal density n_1, n_2 and coupling loss factor η_{12}, η_{21} satisfy the following relationship:

$$n_1\eta_{12} = n_2\eta_{21} \tag{10}$$

Substituting equation (10) into equation (8) and (9), the power balance equations of two subsystems is obtained:

$$\omega\begin{bmatrix}\eta_1+\eta_{12}-\eta_{21} & -\eta_{21}\\ -\eta_{12} & \eta_2+\eta_{21}\end{bmatrix}\begin{Bmatrix}E_1\\E_2\end{Bmatrix} = \begin{Bmatrix}p_1\\p_2\end{Bmatrix} \tag{11}$$

The energy of each system is available from equation (11) and other dynamic responses will be acquired as well. Supposing that SEA model consists of n subsystems, the power balance equation under steady-state conditions of each subsystem can be written as

$$\begin{bmatrix}P_1\\P_2\\\vdots\\P_n\end{bmatrix} = \omega\begin{bmatrix}\eta_{11} & -\eta_{12} & \cdots & -\eta_{n1}\\ -\eta_{12} & \eta_{22} & \cdots & -\eta_{n2}\\ \vdots & \vdots & \vdots & \vdots\\ -\eta_{1n} & -\eta_{21} & \cdots & \eta_{nn}\end{bmatrix}\begin{bmatrix}E_1\\E_2\\\vdots\\E_n\end{bmatrix} \tag{12}$$

$$\eta_{ii} = \eta_i + \sum_{j=1,j\neq i}^{n}\eta_{ij} \tag{13}$$

where P_i, E_i and η_i are the input power, the stored energy and internal loss factor of subsystem i respectively, η_{ij} is the coupling loss factor between subsystem i and j, ω is the one-third- octave band-center frequency.

The energy of each subsystem is obtained from equation (12). The subsystem energy can also be expressed using vibration velocity and pressure

$$E = M < v^2 >= \frac{M < p^2 >}{{Z_o}^2} \tag{14}$$

where M is the mass of the subsystem, $< v^2 >$ is the mean-square value of spatial vibration velocity, $< p^2 >$ is the mean-square value of spatial sound pressure and Z_o is acoustic impedance. The vibration velocity and sound pressure can be calculated through equation (14).

2.3.2 SEA Model

SEA analysis models are established with VA One for the numerical calculation of fill effect at medium and high frequencies. Firstly, finite element models of the fairing and payloads are built according to structure parameters, then the fairing, payload and brackets are divided into several statistical energy subsystems in SEA model. The SEA model of the fairing filled with the large payload is shown in Figure 7 and Figure 8 shows the point, line and surface connections of fairing/payload combination. The involved frequency range is 250Hz~8000Hz.

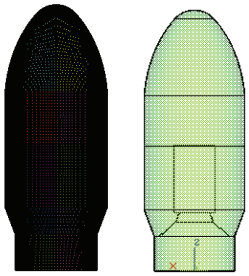

Figure 7 - FE model and SEA model Figure

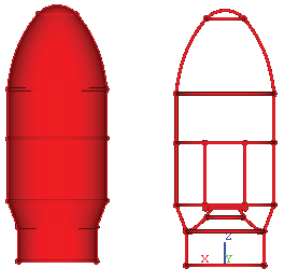

8 - Point, line and surface connections of payload/fairing combination

It is demanded to set up the structure loss factors in SEA model. However, the internal loss factor

mechanism is so complex that it is not easy to obtain them theoretically. An available method to obtain them is experimental measurement. Here, empirical values as 0.1 for the structures and 0.01 for the air cavity are considered in calculation.

The sound source excitation is imposed to the subsystems through diffuse sound field, as shown in Figure 9.

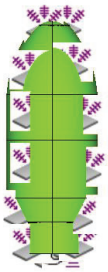

Figure 9 - Schematic of imposed acoustic load

Figure 10 - Test acoustic chamber and payload fairing

3. ACOUSTIC TEST AND LOAD CONDITION

Acoustic tests are carried out in a reverberant acoustic field with a volume of 4000m^3, as shown in Figure 10. The frequency range measured is 31.5Hz~8000Hz (band-center frequency). The sound pressure is measured by using microphones located interior and exterior the fairing, including 19 measuring ones and 4 control ones. Figure 11 displays the location of these microphones. The two excitation conditions are given in table 2, the total SPL are 141.5dB and 146.5dB. The exterior sound field distribution under two acoustic excitation conditions is shown in Figure 12. It is found that a differences between the actual SPLs and the input values, which may be associated with the control state of the experimental equipment (the speaker diaphragm position for example). In that case, it is required for repetitive correction when calculating the fill effect.

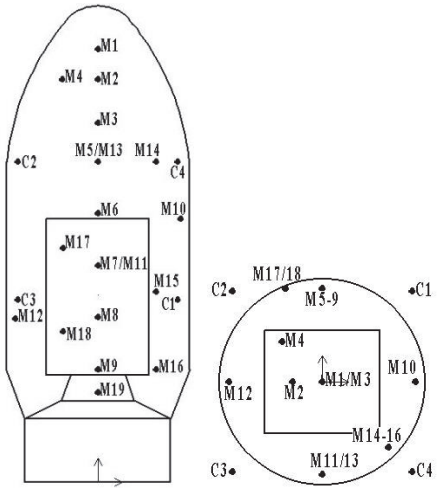

Figure 11 - Microphone locations

Table 2 - Reverberation chamber incentives SPL (octave)

frequency /Hz	SPL（dB）		frequency /Hz	SPL（dB）	
	141.5	146.5		141.5	146.5
31.5	120.5	125.5	630	128.4	133.4
40	123.6	128.6	800	125.3	130.3
50	123.5	128.5	1000	123.4	128.4
63	126.5	131.5	1250	124.3	129.3
80	129.6	134.6	1600	124.1	129.1
100	133	138	2000	123.2	128.2

125	134.2	139.2	2500	121.1	126.1
160	128.8	133.8	3150	120.6	125.6
200	127.3	132.3	4000	118.9	123.9
250	128.3	133.3	5000	117.5	122.5
315	129.3	134.3	6300	117.6	122.6
400	129.2	134.2	8000	118.2	123.2
500	131.3	136.3			

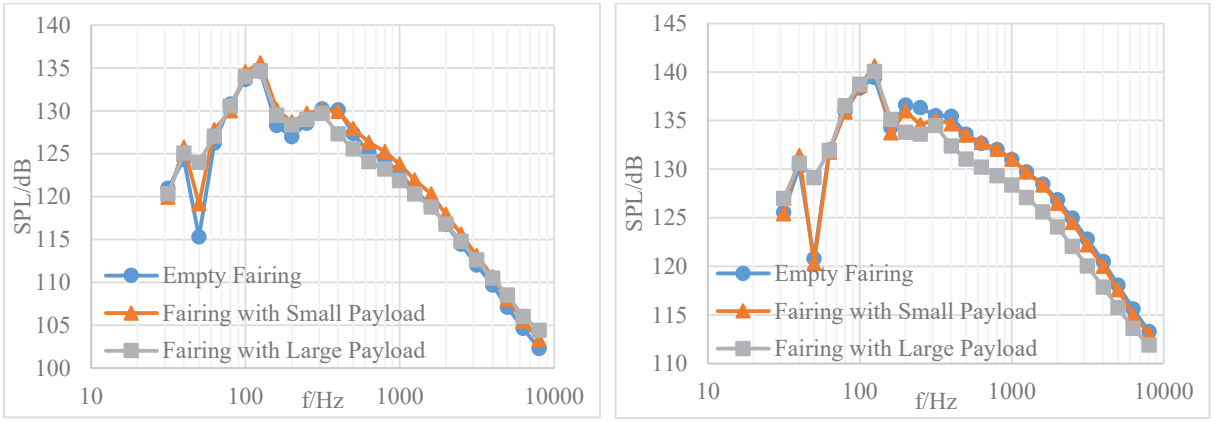

(a) Total SPL 141.5dB (b) Total SPL 146.5dB

Figure 12 - Exterior SPL distribution of different conditions

4. RESULTS ANALYSIS AND DISCUSSION

4.1 Simulation and Test Results Comparison

During a rocket launch, the main problem concerned is the sound field environment around the payload. Fill effect is calculated through the change of average interior SPL for the cavity between payload and firing. Figure 13 and Figure 14 are the measured and simulation fill effects of the two payloads under different test conditions. It can be seen that the simulation values are in agreement with the experimental data. The fill effect has a wide fluctuation range at low frequencies and gradually approaches zero as frequency increases. Moreover, it becomes negative values at some frequencies. When the excitation total SPL is 146.5dB, the fill effect of the large payload obtained by simulation and experiment are 8.24dB, 12.37dB, and that of the small payload are 3.78dB and 5.47dB respectively. Under 141.5dB, the fill effect of the large payload obtained by simulation and experiment are 9.25dB, 7.45dB respectively and that of the small payload are 3.15dB and 5.49dB respectively. It is illustrated that SPL changes inside the fairing due to payload filling are extremely obvious, especially at lower frequencies, which will impose additional acoustic loads to the fairing, the payload or other devices and accelerate structural damages.

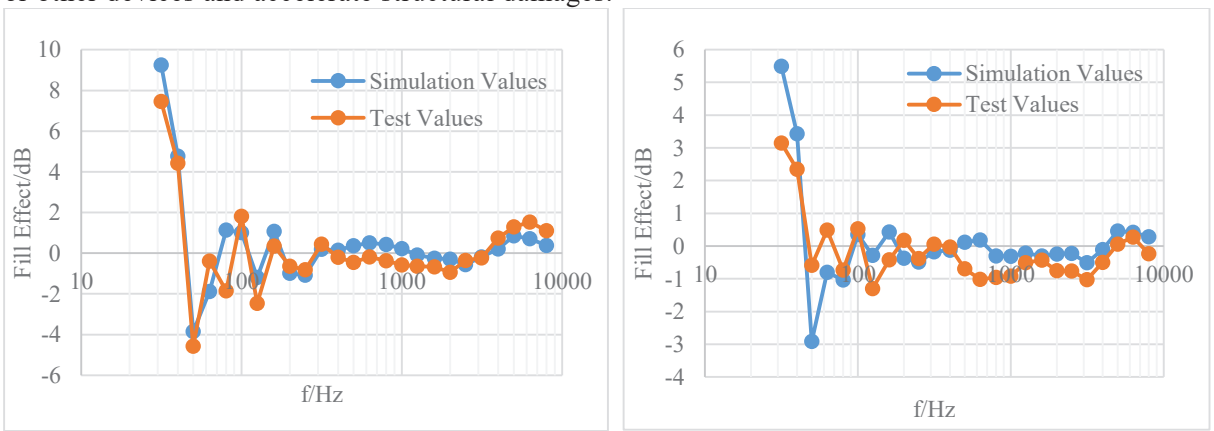

(a) Fill effect comparison of large payload (b) Fill effect comparison of small payload

Figure 13 - Fill effect comparison of total SPL 146.5dB

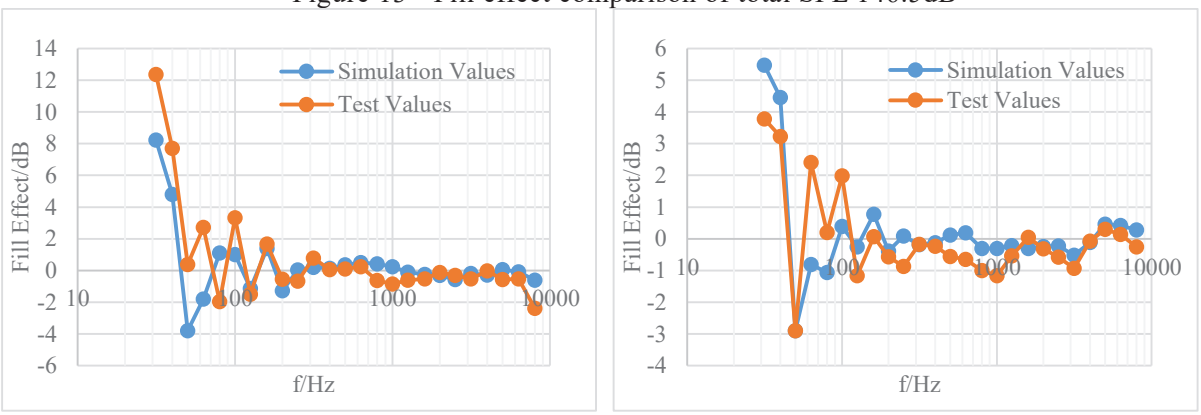

(a) Fill effect comparison of large payload (b) Fill effect comparison of small payload

Figure 14 - Fill effect comparison of total SPL 141.5dB

It is demonstrated in NASA standard that different payload fill factor causes different fill effects. The fill effect comparison of the two payloads are summarized in Figure 15 and 16, as we can see, the values of the large payload with a bigger fill factor are almost larger. The fill effect difference from simulation result is 4dB, while it is up to 8dB from test result. That shows the difference caused by the payload fill factor change is significant, which is possibly a factor that we must take into account and use different criteria in structure design of various payloads.

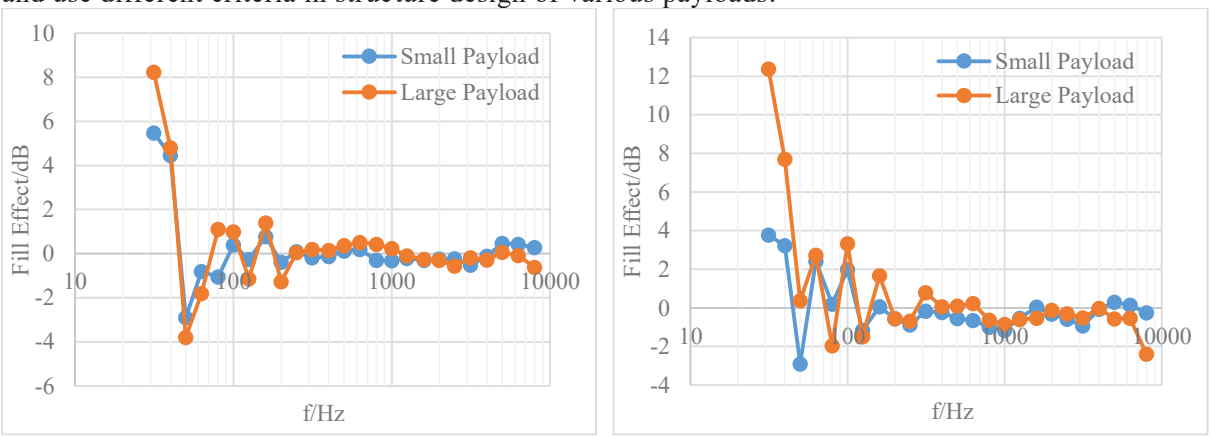

(a) Comparison of simulation values (b) Comparison of test values

Figure 15 – Fill effect comparison of total SPL 146.5dB

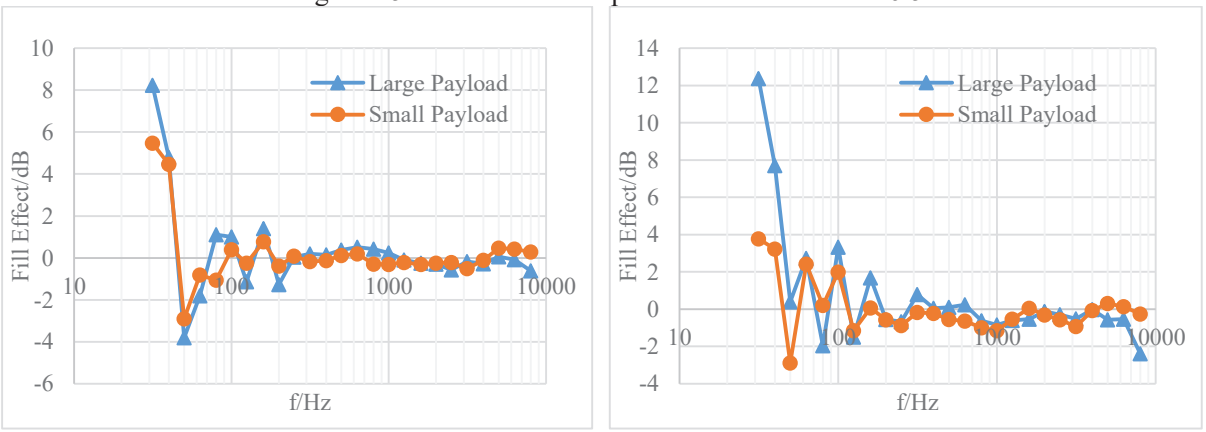

(a) Comparison of simulation values (b) Comparison of test values

Figure 16 - Fill effect comparison of total SPL 141.5dB

4.2 Analysis of Acoustic Natural Frequencies Shifts

To study the mechanism and characteristics of fill effect, the coupled acoustic modes of the clearance gap cavity between the fairing and payload are analyzed. Table 3 presents the first ten

natural frequencies of the gap cavity under different test conditions. It can be seen that two modes are inserted between the second (22.4669Hz) and the third mode (42.2256Hz) of the empty fairing .And the original 3st~5th mode shapes of the cavity are changed as well. The two modes at 48.7Hz of the empty fairing shift to lower frequencies, 39.07Hz and 40.66Hz with small payload, 36.77Hz and 38.60Hz with large payload, which causes the SPL decrease at 50Hz 1/3 octave band after payload is filled in. That's why the fill effect curves of two payloads have a negative valley at 50Hz. And maybe the fluctuation of positive and negative values of the fill effect can be explained in that way.

Table 3 - First ten natural frequencies of the gap cavity under different conditions

Payloads / Number	No Payload	Small Payload	Large Payload
1	0.0001	0.0001	0
2	22.4669	21.995	20.772
3	42.2256	39.076	36.773
4	48.7379	40.668	38.601
5	48.7493	41.385	41.380
6	56.5653	54.341	52.261
7	56.5770	54.500	52.651
8	60.0886	59.644	57.330
9	70.4134	67.118	64.408
10	70.4464	67.551	65.363

For the other nonzero frequencies of the first ten modes, the frequency of the same mode shifts to the lower stage as the payload fills in. And bigger shift ratio comes out with a larger fill factor, which results in higher modal density in a specific band at low frequencies. In that way, average the SPL in the fairing becomes higher with a larger fill factor, and the fill effect is about to be more obvious simultaneously.

5. CONCLUSIONS

In this paper, the numerical analysis models for the firing with payloads are established using FE-BEM and SEA method to carry out numerical computation of fill effect at low and high frequencies respectively, and the fill effects of the firing with small and large payload are investigated and tested. Conclusions can be summarized:

1) The payload fill effect at low frequencies is computed using FE-BEM method, simulation and test results show that the fill effect is more obvious at low frequencies. It has a wide range of fluctuation with positive and negative values. Maximum fill effect of the large payload is up to 12.4dB and the variation range is about 16dB. Maximum fill effect of the small payload is up to 5.5dB and the variation range is about 8.5dB. The SPL changes inside the fairing are extremely obvious due to payload filling at lower frequencies, which will impose additional acoustic loads to the fairing, the payload or other devices and accelerate structural damages.

2) The payload fill effect at medium and high frequencies is computed using SEA method, simulation and test results show that, the fill effect is not big and nearly about zero. The fluctuation range are 1.5dB~-2.3dB and 0.46dB~-1.1dB respectively for the large and small payload. As the simulation and test values show similar distribution pattern, it's illustrated that SEA method can accurately predict fill effect of different payloads at medium and high frequencies.

3) New acoustic modes appear and original natural frequencies shift due to payload fills in the fairing, which leads to obvious fill effect and wide fluctuation range with positive and negative values at low frequencies, while the fill effect is about zero at high frequencies. Because different payload fill factor results in different frequency shift ratio, the fill effect will be more obvious with a larger payload fill factor. The change rules can be predicted by numerical computation method, so as to provide basis for the establishment of ground acoustic test conditions about payload.

ACKNOWLEDGEMENTS

This work is supported by Natural Science Foundation of China (Grant No. 50775225), Open Research Foundation of State Key Laboratory of Vehicle NVH and Safety Technology (Grant No. NVHSKL201405) and Open Research Foundation of Science and Technology on Reliability and

Environmental Engineering Laboratory (Grant No. KHZS20153001). These financial supports are acknowledged greatly.

REFERENCES

1. William O. Hughes and Mark E. McNelis .NASA LeRC's Acoustic Fill Effect Test Program and Results. NASA Technical Memorandum 106688.
2. Terry Scharton. The Fill Factor, Fact or Fiction[C]//The 2005 Spacecraft & Launch Vehicle Dynamics Environment Workshop. 2005.
3. Nagahama K, Ando S, Shi Q, et al. Vibra-acoustic analysis of narrow cavity effect of satellite at launch[C]//Spacecraft Structures, Materials and Mechanical Testing 2005. 2005, 581: 77.
4. Engberg T, Korde U A. Acoustic Modeling of Rocket Payload Bays Withing Launch Fairings[D]. South Dakota School of Mines and Technology, Rapid City, 2011.
5. Gruszka K, Nabiałek M, Szota M. The influence of fill factor on the phononic crystal eigenfrequencies [J]. 2014.
6. Burton W S, Noor A K. Assessment of continuum models for sandwich panel honeycomb cores [J]. Computer methods in applied mechanics and engineering, 1997, 145(3): 341-360.
7. Saidi A, Coorevits P, Guessasma M. Homogenization of a sandwich structure and validity of the corresponding two-dimensional equivalent model [J]. Journal of Sandwich Structures and Materials, 2005, 7(1): 7-30.
8. Jinsen Zhao. Research on Equivalent Models of the Mechanical Function for Aluminum Honeycomb Sandwich Panel [D]. Nanjing, Nanjing University of Aeronautics & Astronautics, 2006.
9. Tieliang Zhang, Yunliang Ding, Haibo Jin. Comparative analysis of equivalent models for honeycomb sandwich plates [J]. Chinese Journal of Applied Mechanics, 2011, 28(3): 275-282.
10. LI X, WEN J, YU D, et al. THE COMPARATIVE STUDY OF EQUIVALENT MECHANICAL METHODS ON HONEYCOMB SANDWICH PLATE[J]. Fiber Reinforced Plastics, 2012: S1.
11. Yuchao Yang. Analysis and Verification of Composite Plates SEA Model [D]. Harbin Institute of Technology, 2013.
12. Wang J, Zhang J H, Ning W. Sound-vibration coupling analysis under combined environment [J]. Zhendong yu Chongji(Journal of Vibration and Shock), 2011, 30(2): 15-18.
13. W Desmet, P Sas, D Vandepitte - LMS International, 1998.
14. Deyuan Yao, Qizheng Wang. Mechanism and Application of SEA Analysis [M]. Beijing, Beijing Institute of Technology Press, 1995.
15. Shuming Chen. Research on Prediction and Control Methods of Automobile Middle and High Frequency Noise [D] [D]. Jilin University, 2011.